


# SCIENTIFIC REPORTS



OPEN

## Erbium-doped fiber laser passively mode locked with few-layer WSe<sub>2</sub>/MoSe<sub>2</sub> nanosheets

Dong Mao<sup>1,2</sup>, Xiaoyang She<sup>1,2</sup>, Bobo Du<sup>1,2</sup>, Dexing Yang<sup>1,2</sup>, Wending Zhang<sup>1,2</sup>, Kun Song<sup>2</sup>, Xiaoqi Cui<sup>1,2</sup>, Biqiang Jiang<sup>1,2</sup>, Tao Peng<sup>1,2</sup> & Jianlin Zhao<sup>1,2</sup>

Received: 05 January 2016

Accepted: 09 March 2016

Published: 24 March 2016

Few-layer transition-metal dichalcogenide WSe<sub>2</sub>/MoSe<sub>2</sub> nanosheets are fabricated by a liquid exfoliation technique using sodium deoxycholate bile salt as surfactant, and their nonlinear optical properties are investigated based on a balanced twin-detector measurement scheme. It is demonstrated that both types of nanosheets exhibit nonlinear saturable absorption properties at the wavelength of 1.55 μm. By depositing the nanosheets on side polished fiber (SPF) or mixing the nanosheets with polyvinyl alcohol (PVA) solution, SPF-WSe<sub>2</sub> saturable absorber (SA), SPF-MoSe<sub>2</sub> SA, PVA-WSe<sub>2</sub> SA, and PVA-MoSe<sub>2</sub> SA are successfully fabricated and further tested in erbium-doped fiber lasers. The SPF-based SA is capable of operating at the high pump regime without damage, and a train of 3252.65 MHz harmonically mode-locked pulses are obtained based on the SPF-WSe<sub>2</sub> SA. Soliton mode locking operations are also achieved in the fiber laser separately with other three types of SAs, confirming that the WSe<sub>2</sub> and MoSe<sub>2</sub> nanosheets could act as cost-effective high-power SAs for ultrafast optics.

Two-dimensional layered materials have attracted increasing attention from fundamental researches to industrial applications attributing to their unique dimensionality effect as well as outstanding physical/chemical property<sup>1–4</sup>. Graphene, the most famous two-dimensional material, possesses a Dirac-like electronic band structure, enabling ultra-broadband response ranging from ultraviolet to terahertz<sup>5</sup>. Since the few- and single-layer graphene was fabricated by the micromechanical cleavage method, it has been in-depth studied and applied in fields of photon detection, graphene plasmonics, ultrafast optics, quantum electrodynamics, *et al.*<sup>6–9</sup>. However graphene also suffers the deficiency of the weak absorption coefficient (2.3% of incident light per layer), which limits its modulation ability and potential applications. In addition to graphene, transition-metal dichalcogenides (TMDs), a family of inorganic two-dimensional layered materials with the chemical formula of MX<sub>2</sub>, where M is a transition metal (usually Mo, W) and X is a group VI element (S, Se, Te), are attracting continuously rising interest due to its exotic physical properties such as non-zero bandgap and layer-dependent second-order optical nonlinearity<sup>10–13</sup>. The in-plane atoms of TMD materials are held together by strong chemical bonds while weak Van der Waals interaction enables stacking between layers, which enables them to be exfoliated into thin nanosheets for developing high-performance optoelectronic devices<sup>14,15</sup>.

Molybdenum disulfide (MoS<sub>2</sub>) and tungsten disulfide (WS<sub>2</sub>), two representative TMDs, received the most research attention during the past several years<sup>16–18</sup>. In the branch of optics, a great deal of research interest is focused on the nonlinear saturable absorption property of MoS<sub>2</sub> and WS<sub>2</sub> nanosheets<sup>19–23</sup>. Wang *et al.* reported that few-layer MoS<sub>2</sub> display ultrafast saturable absorption property at 515 nm and 800 nm<sup>20</sup>, and observed the strong two-photon absorption and saturable absorption respectively in mono- as well as multi-layer MoS<sub>2</sub> at 1030 nm<sup>24</sup>. By the introduction of sulfur defects in MoS<sub>2</sub>, Yu *et al.* found that the bandgap of MoS<sub>2</sub> nanosheets can be significantly reduced, and realized a broadband saturable absorber (SA) achieving Q-switched lasers at 1.06, 1.42, and 2.1 μm<sup>21</sup>. Recently, several groups including us demonstrated that WS<sub>2</sub> nanosheets exhibit broadband saturable absorption property even at sub-bandgap photon energies<sup>25,26</sup>. Hereafter, various types of MoS<sub>2</sub> or WS<sub>2</sub> SAs were proposed to realize passively mode-locked or Q-switched lasers<sup>26–29</sup>.

<sup>1</sup>Shaanxi Key Laboratory of Optical Information Technology, School of Science, Northwestern Polytechnical University, Xi'an 710072, China. <sup>2</sup>Key Laboratory of Space Applied Physics and Chemistry, Ministry of Education, School of Science, Northwestern Polytechnical University, Xi'an 710072, China. Correspondence and requests for materials should be addressed to D.M. (email: maodong@nwpu.edu.cn)

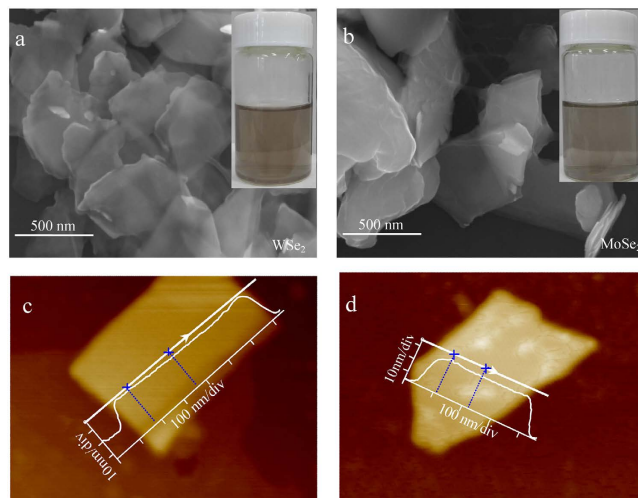


**Figure 1. Characterization of WSe<sub>2</sub>/MoSe<sub>2</sub> nanosheets.** SEM images (a,b) and AFM images (c,d). The inset of Fig. 1(a,b) shows the corresponding suspensions of the nanosheets.

In comparison with MoS<sub>2</sub> and WS<sub>2</sub>, molybdenum diselenide (MoSe<sub>2</sub>) and tungsten diselenide (WSe<sub>2</sub>) exhibit the similar molecular structure while have smaller optical bandgaps. For instance, the bandgaps of bulk MoS<sub>2</sub> and WS<sub>2</sub> are 1.29 and 1.35 eV while that of MoSe<sub>2</sub> and WSe<sub>2</sub> are 1.09 and 1.2 eV respectively<sup>30</sup>. This special bandgap is particularly interesting for laser applications from the visible to near-infrared wavelength regime<sup>31–33</sup>. Luo *et al.* demonstrated a compact red-light Q-switched praseodymium-doped all-fiber laser using two-dimensional TMDs as SAs<sup>34</sup>. However, the study of WSe<sub>2</sub> and MoSe<sub>2</sub> is mainly concentrated on fabrication method and electronic property<sup>32,35</sup> and their nonlinear optical behavior still remains less addressed up till now. We think that the investigation of emerging saturable absorption material is a key step for developing its potentials. In this contribution, we prepare WSe<sub>2</sub> and MoSe<sub>2</sub> nanosheets with a liquid exfoliation method using sodium deoxycholate bile salt as surfactant. Experimental results demonstrate that both WSe<sub>2</sub> and MoSe<sub>2</sub> nanosheets display saturable absorption property at the wavelength of 1.55 μm. By utilizing SPF- and PVA-based WSe<sub>2</sub>/MoSe<sub>2</sub>-SAs, stable picoseconds soliton pulses are delivered from the erbium-doped fiber (EDF) laser separately, including a train of 3252.65 MHz harmonically mode-locked ultrafast pulses.

## Results

**Preparation and characterization of WSe<sub>2</sub>/MoSe<sub>2</sub> SAs.** Various techniques have been explored to prepare mono- or few-layer TMD nanosheets, such as chemical vapor deposition, micromechanical exfoliation, liquid exfoliation, *et al.*<sup>11</sup>. Each method has its advantages and ranges of applications. For example, micromechanical exfoliation is capable of producing high-quality nanosheets, while the production efficiency and size are limited. Chemical vapor deposition could synthesize large-scale mono- or few-layer TMD films. However, the synthetic process is quite complicated and requires high temperature. Liquid exfoliation is a simple and cost-effective method to produce mass dispersions of mono- and few-layer TMD nanosheets or other two-dimensional materials at ambient conditions<sup>36,37</sup>. Here, the WSe<sub>2</sub>/MoSe<sub>2</sub> nanosheets are prepared by the liquid exfoliation method, which is similar to that of previous reports<sup>36</sup>.

The insets of Fig. 1(a,b) show the suspensions of WSe<sub>2</sub>/MoSe<sub>2</sub> nanosheets, which display faint red color for WSe<sub>2</sub> and slight grey for MoSe<sub>2</sub> respectively. These suspensions are quite stable, and display no aggregation after being stored for several weeks under ambient conditions. The nanosheets are characterized by scanning electron microscope (SEM), as illustrated in Fig. 1(a,b). Both WSe<sub>2</sub> and MoSe<sub>2</sub> are present as two-dimensional nanosheets with intact surface texture, confirming successful exfoliation of the bulk-state crystal. The length and width of most nanosheets are below 1 μm, which depends on the centrifugation rate during the fabrication. The atomic force microscope (AFM) image illustrate that the thickness of nanosheets is ~20 nm for WSe<sub>2</sub> and ~15 nm for MoSe<sub>2</sub>, as illustrated in Fig. 1(c,d). Based on above results, one can convince that the WSe<sub>2</sub>/MoSe<sub>2</sub> nanosheets are successfully fabricated using the proposed method.

After the successful exfoliation of the bulk crystal, we then fabricate two types of WSe<sub>2</sub>/MoSe<sub>2</sub>-based SAs and investigate their saturable absorption properties. The first type of SA is obtained by depositing the WSe<sub>2</sub>/MoSe<sub>2</sub> nanosheets onto a side polished fiber (SPF) to realize mutual interaction of nanosheets with the evanescent field of light within the SPF. The SPF is fabricated by polishing a bent single-mode fiber (SMF) on one side. The depth between the polished surface and fiber core of SPF is about 2 μm, and the polished part of the fiber has a length of 1.2–1.5 mm. Then the WSe<sub>2</sub>/MoSe<sub>2</sub> nanosheets dispersion is dropped on the surface of SPF that is fixed on a quartz plate. At last, a 10 mW 1.55 μm continuous wave is coupled into the SPF and the optical deposition process starts. The deposited length and depth depend on the deposition time and input power, and the insertion loss is monitored in real time with an optical power meter. Actually, the insertion loss of the SA should be moderate, for example, mode locking operation can be achieved when the insertion loss ranges from 20% to 80%. By virtue of lateral interaction scheme, the TMD nanosheets interact with light over long distance while experience low intensity, which allows the SA to work at the high-power regime. Figure 2(a,b) shows the SPF deposited with

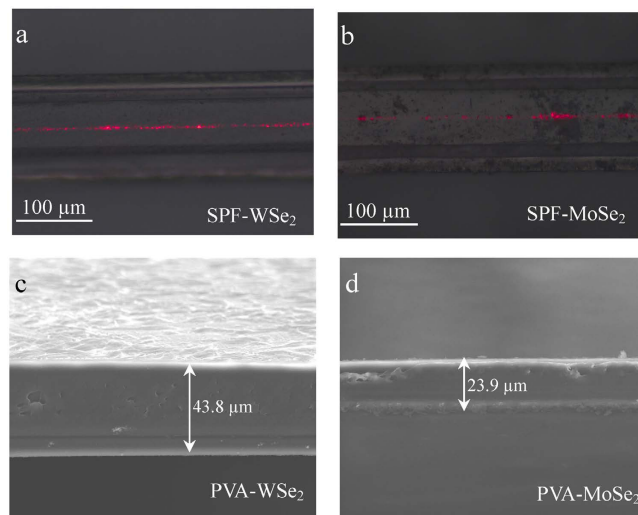


**Figure 2.** Optical micrograph of SPF deposited with WSe<sub>2</sub> nanosheets (a) and MoSe<sub>2</sub> nanosheets (b). Side profile of WSe<sub>2</sub>-PVA film (c) and MoSe<sub>2</sub>-PVA film (d).

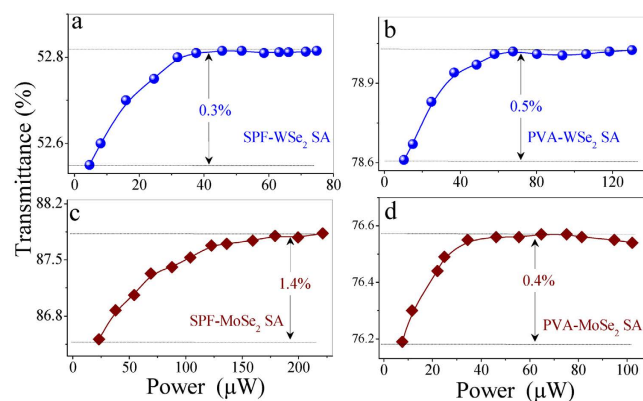


**Figure 3.** Nonlinear transmissions of SPF-WSe<sub>2</sub> SA (a), PVA-WSe<sub>2</sub> SA (b), SPF-MoSe<sub>2</sub> SA (c), and PVA-MoSe<sub>2</sub> SA (d).

WSe<sub>2</sub>/MoSe<sub>2</sub> nanosheets after injecting a 632.8 nm He-Ne laser. The red laser is scattered from the surface of the SPF, indicating the existence of evanescent light field.

The other type of SA is fabricated by mixing the WSe<sub>2</sub>/MoSe<sub>2</sub> nanosheets with aqueous PVA solution and evaporating the mixture on a substrate. This process could be described as follows. First, 5 Wt% PVA solution and the WSe<sub>2</sub>/MoSe<sub>2</sub> dispersions are mixed at a volume ratio of 1:3 by a magnetic stirrer for 5 hours. Then, a thin WSe<sub>2</sub>/MoSe<sub>2</sub>-PVA film is formed by evaporating the mixture on a quartz plate under ambient temperature and pressure for 48 hours. At last, the film is cut into small pieces ( $\sim 1 \times 1$  mm) and sandwiched between two facets of a fiber connector to realize fiber-based SA. The thicknesses of WSe<sub>2</sub>/MoSe<sub>2</sub>-PVA film are measured as 43.8 and 23.9  $\mu\text{m}$ , as shown in Fig. 2(c,d), respectively. Compared with optical deposition<sup>38</sup> or dropping nanosheets on quartz plate<sup>39</sup>, the PVA-film method would be more attractive due to its advantages of controllability, flexibility, and cost-effectiveness.

Based on a balanced twin-detector measurement method<sup>40</sup>, we investigate the nonlinear saturable absorption property of four SAs (SPF-WSe<sub>2</sub>, PVA-WSe<sub>2</sub>, SPF-MoSe<sub>2</sub>, and PVA-MoSe<sub>2</sub>). Figure 3(a,d) shows the saturable absorption data of the WSe<sub>2</sub>/MoSe<sub>2</sub> SA as a function of pulse power. One can observe that the transmission efficiencies of four SAs increase with pulse intensity, which is the typical characteristic of nonlinear saturable absorption. The modulation depths of SPF-WSe<sub>2</sub> and PVA-WSe<sub>2</sub> SAs are given as 0.3% and 0.5%, and that of the MoSe<sub>2</sub> are given as 1.4% and 0.4%. During the experiment, we did not observed nonlinear response from other devices, which suggest that the saturable absorption property is purely caused by TMD nanosheets. The proposed SAs may find wide applications in ultrafast photonics, including high-speed light modulation, optical switching, and ultrashort pulse generation.

**Setup of WSe<sub>2</sub>/MoSe<sub>2</sub> mode locked fiber laser.** Fiber lasers possess inherent advantages of alignment-free operation, excellent beam quality, high efficiency<sup>41,42</sup>, which provides an ideal platform to study the nonlinear optical property of new emerging materials such as carbon nanotube<sup>40,43</sup>, graphene<sup>6,43,44</sup>, topological

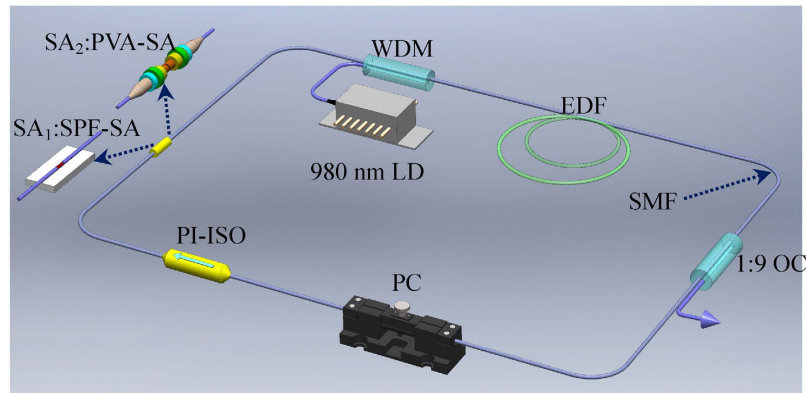


**Figure 4. Schematic of the passively mode-locked fiber laser based on  $\text{WSe}_2/\text{MoSe}_2$  SAs.**  $\text{SA}_1$  and  $\text{SA}_2$  are SPF- and PVA-based SAs, respectively. Wavelength division multiplexer (WDM); Erbium-doped fiber (EDF); Output coupler (OC); Single-mode fiber (SMF); Polarization controller (PC); Polarization insensitive isolator (PI-ISO).

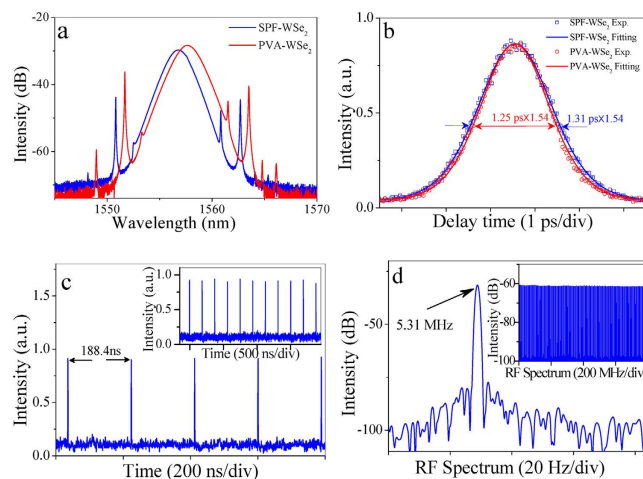


**Figure 5. Output characteristics of  $\text{WSe}_2$  mode-locked fiber laser.** (a) optical spectrum, (b) autocorrelation trace, (c) pulse train, and (d) RF spectrum. The inset shows the broadband RF spectrum at a span of 800 MHz.

insulator<sup>39</sup>, black phosphorus<sup>45,46</sup>, and TMDs<sup>28</sup>. Here, we construct an EDF laser to further test the saturable absorption property of four different SAs. The fiber resonator is composed of a 6 m EDF with 3 dB/m absorption at 980 nm, a fiber fused coupler with the output ratio of 10%, a polarization insensitive isolator, a SA, and a polarization controller, as shown in Fig. 4. The EDF used in the fiber laser is EDFC-980-HP, which has a mode field diameter of  $5.8 \pm 0.5 \mu\text{m}$  and doping concentration of 1500 ppm. A 980 nm laser diode with the maximum power of 610 mW is used to pump the EDF via a wavelength-division multiplexer. The polarization controller can adjust the polarization state of the laser, but it is not fundamental to realize the mode locking operation. The pigtailed  $\text{WSe}_2$  SA and  $\text{MoSe}_2$  SA are 0.7 and 2.8 m, respectively. The other fiber is SMF with a total length of 32 m. Considering the dispersion parameters  $D$  of  $-16 \text{ ps}/(\text{nm}\cdot\text{km})$  and  $17 \text{ ps}/(\text{nm}\cdot\text{km})$  for EDF and SMF, the net dispersion  $\beta_2$  of the fiber laser is calculated as  $-0.59 \text{ ps}^2$  for  $\text{WSe}_2$  SA and  $-0.63 \text{ ps}^2$  for  $\text{MoSe}_2$  SA, which facilitates soliton pulse shaping through the interaction of self-phase modulation and anomalous group velocity dispersion.

**Experimental observations.** We first investigate the mode-locking performance of the fiber laser by inserting the SPF- $\text{WSe}_2$  SA into the cavity. At the pump power of 21 mW, self-starting soliton mode locking operation is achieved with the output power of 0.45 mW. As illustrated by the blue curve in Fig. 5(a), the output spectrum is centered at 1556.7 nm with a 3-dB bandwidth of 2 nm. Several pairs of sidebands are symmetrically distributed in the optical spectrum, which is the typical characteristic of standard soliton. The pulse duration is measured by a high-sensitivity commercial autocorrelator. The autocorrelation trace has a full width at half maximum of 2 ps, as shown by the blue curve in Fig. 5(b). By using a  $\text{Sech}^2$  fitting, the pulse duration is estimated to be 1.31 ps. During the experiment, the fiber laser tended to operate at multiple-pulses state due to the combined effects of soliton energy quantization and long cavity length<sup>47</sup>. However, taking hysteresis phenomena of the soliton fiber laser, single-pulse mode locking can be obtained by slowly decreasing the pump power to 13 mW. The oscilloscope trace of the output pulse train is demonstrated in Fig. 5(c), which gives the pulse interval of 188.4 ns, well consistent with the cavity length of 38.7 m. The offset from zero position of y-axis on the oscilloscope trace may be

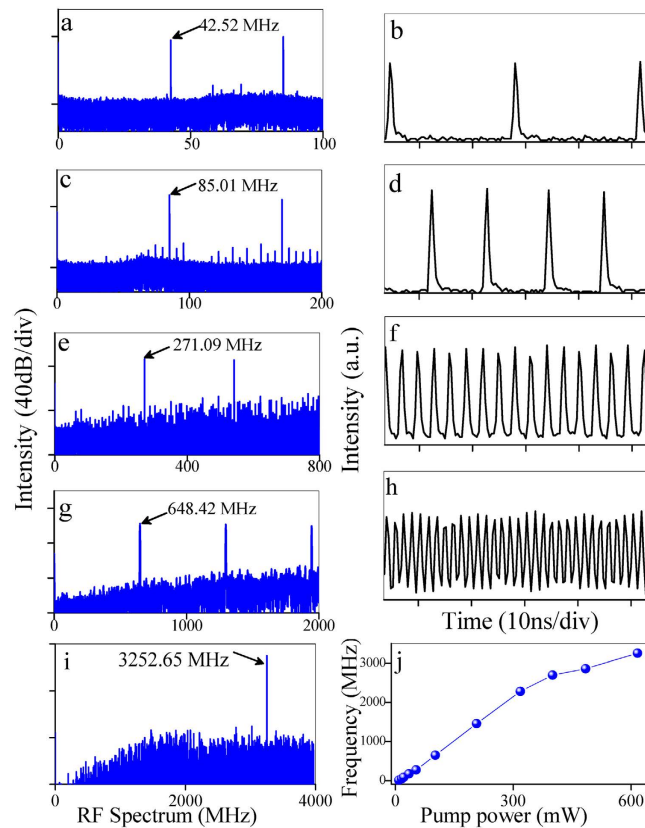


**Figure 6.** Harmonically mode-locked fiber laser based on the SPF-WSe<sub>2</sub> SA. RF spectrum (a,c,e,g,i) and pulse train (b,d,f,h); (j) Frequency of output pulses as a function of the pump power.

attributed to the combined effects of weak input power and continuous wave of the sidebands. The fundamental repetition rate of the pulse is given as 5.31 MHz, as shown in Fig. 5(d). The inset shows the broadband RF spectrum at a span of 800 MHz. To verify whether the mode locking is induced by WSe<sub>2</sub> nanosheets, we have replaced the SPF-WSe<sub>2</sub> SA by the PVA-WSe<sub>2</sub> SA in the cavity. In this case, soliton mode locking operation is also observed in the fiber laser at the pump of 35 mW. The optical spectrum and autocorrelation trace of the pulses are demonstrated by red curves in Fig. 5(a,b), respectively. Here, the output power of the fiber laser is measured as 0.84 mW, and the pulse evolution and radio frequency (RF) spectrum are quite similar with that of SPF-WSe<sub>2</sub> mode-locked fiber laser, which are not present in the text for conciseness.

Apart from the single- or multi-pulses operation reported previously, harmonic mode locking is also observed in the SPF-WSe<sub>2</sub> mode locked fiber laser. We use a 27.5 GHz RF analyzer with a 45 GHz photodetector to directly monitor the repetition rate of the output pulses. As shown in Fig. 6(a–i), by increasing the pump power from 25 to 610 mW, the repetition rate of the pulses gradually increases from 42.52 to 3252.65 MHz (612<sup>th</sup> harmonic of fundamental repetition frequency), and the output power increases from 0.6 to 19 mW. Due to the bandwidth limitation (500 MHz), the 3252.65 MHz pulses cannot be displayed correctly on the used oscilloscope. Figure 6(j) summarizes the evolution of the pulse repetition rate as a function of the pump power. The repetition rate almost changes linearly at low pump power. Actually, the maximum pulse repetition rate is limited by the available pump power and can be further enhanced by optimizing the SA, such as using fiber-taper based SAs. The formation mechanism of harmonic mode locking can be attributed to long-period interaction between solitons<sup>48</sup>. When the solitons and non-soliton components exhibit certain phase difference, the interaction force becomes repulsive for all solitons within a pulse bunch and results in uniform distributed pulses inside the laser cavity. Such high-repetition-rate pulsed fiber laser can find important applications such as frequency combs and soliton communications.

As the extra heating can be rapidly dissipated from the SPF, the SPF-WSe<sub>2</sub> SA can work at mode locking state at the pump power of 600 mW during the whole experiment (about four hours). Using bidirectional pump scheme with the total pump power of 1.2 W, the fiber laser can work at mode locking state for several minutes and then evolves into continuous wave state. In this case, the intracavity power is calculated as 400 mW from the output power. However, by decreasing the pump power to zero and then increasing pump power, mode-locking operation can be obtained again. Based on these results, we infer that the damage threshold of the SA is about 400 mW.

By using SPF- and PVA-MoSe<sub>2</sub> SAs, mode-locked operation can also be realized in the fiber laser, similar to that of WSe<sub>2</sub> SA. The blue and red curves show the laser performances based on SPF- and PVA-MoSe<sub>2</sub> SAs respectively, as demonstrated in Fig. 7. The spectral width, pulse interval, pulse duration, and fundamental repetition rate for SPF-MoSe<sub>2</sub> mode-locked pulses are 2.3 nm, 1.09 ps, 198.8 ns, and 5.03 MHz, respectively. The



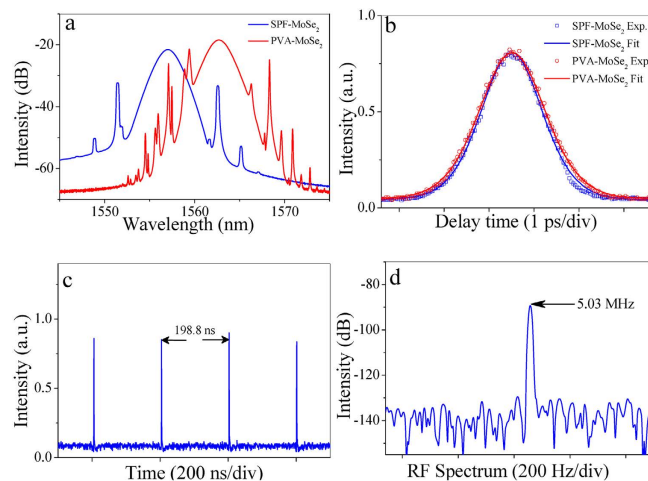


**Figure 7.** Output characteristics of MoSe<sub>2</sub> mode-locked fiber laser. (a) Optical spectrum, (b) autocorrelation trace, (c) pulse train, and (d) RF spectrum.

SA types	SA parameters		Nanosheets parameters		Mode-locked laser performance			
	Modulation depth (%)	Thickness (μm)	Size (μm)	Thickness (μm)	Central wavelength (nm)	Spectral Bandwidth (nm)	Pulse duration (ps)	Repetition Rate (MHz)
SPF-WSe <sub>2</sub>	0.3	//	0.4~1	~15	1556.7	2	1.31	5.31
PVA-WSe <sub>2</sub>	0.5	43.8			1557.6	2.1	1.25	5.31
SPF-MoSe <sub>2</sub>	1.4	//	0.4~1	~20	1557.1	2.3	1.09	5.03
PVA-MoSe <sub>2</sub>	0.4	24.9			1562.6	2.2	1.18	5.03

**Table 1.** Summarization of SA parameters and laser performance.

corresponding time bandwidth product is calculated as 0.316, indicating that the output pulse is a chirp-free soliton. The central wavelength changes for different mode-locking operations, which is mainly attributed to the variation of pump power, insertion loss, and polarization state. Table 1 summarizes the SA parameters and the corresponding laser performance for a clear comparison.

E. M. Pessina *et al.* demonstrated that self-mode locking operation can be achieved due to multimode laser instability<sup>49</sup>. However, the instability-induced mode-locked fiber laser always operates at the fundamental repetition rate and cannot deliver stable picosecond pulses, which is different from our operations. For example, the MoSe<sub>2</sub>/WSe<sub>2</sub> mode-locked fiber laser is capable of generating robust single/multiple pulses without average. Moreover, soliton mode locking operation could be also obtained in a fiber laser with length of 11 m using the proposed SAs. We have carried out comparative experiments to verify whether the mode locking operation is purely caused by WSe<sub>2</sub>/MoSe<sub>2</sub> nanosheets. In the experiment, continuous wave is always observed in the fiber laser by using pure SPF (directly exposed on air), PVA film, or removing the WSe<sub>2</sub>/MoSe<sub>2</sub> SAs, despite that the polarization controller and the pump power are tuned over a full range for hundreds of times. In contrast, mode-locking operation can be easily achieved by depositing the WSe<sub>2</sub>/MoSe<sub>2</sub> nanosheets on SPF or inserting the PVA-WSe<sub>2</sub>/MoSe<sub>2</sub> film into the laser cavity. The comparative results confirm again that the WSe<sub>2</sub>/MoSe<sub>2</sub> SAs are responsible for the mode locking operation of the fiber laser.

## Discussion

We found that the dispersion setting and output ratio of fiber cavity strongly affect the laser operations. For example, mode-locking operation can be easily obtained at large anomalous dispersion regime with output ratio less than 10%. However, pulse operation is difficult to achieve at normal dispersion regime or fiber laser with output ratio larger than 20%. The results could be attributed to the small modulation of the WSe<sub>2</sub>/MoSe<sub>2</sub> SAs. As the normal dispersion induced temporal broadening or output induced-perturbation cannot be compensated by the SA, mode-locking will not be established in the fiber laser. Experimental experiments show that MoSe<sub>2</sub>/WSe<sub>2</sub> nanosheets exhibit saturable absorption at 1.55 μm (0.8 eV), although the photon energy is lower than the bandgap of the material. Several groups have proposed different theories to interpret the sub-bandgap saturable absorption, such as defect-induced bandgap decreasing<sup>21</sup>, coexistence of semiconducting and metallic states<sup>22</sup>, two-photon absorption saturation<sup>24</sup>, and edges state of the materials<sup>50</sup>. However, a unanimity interpretation of the governing mechanism has not been fully established. In the view of defect-state theory, the deviation from perfection in two-dimensional materials is inevitable and will renovate their electronic and optical properties<sup>51</sup>. By the introduction of sulfur defects in MoS<sub>2</sub> or WS<sub>2</sub>, the bandgaps of these materials can be significantly reduced<sup>21,25,52,53</sup>, which may further contribute to the broadband saturable absorption. As these TMD materials possess

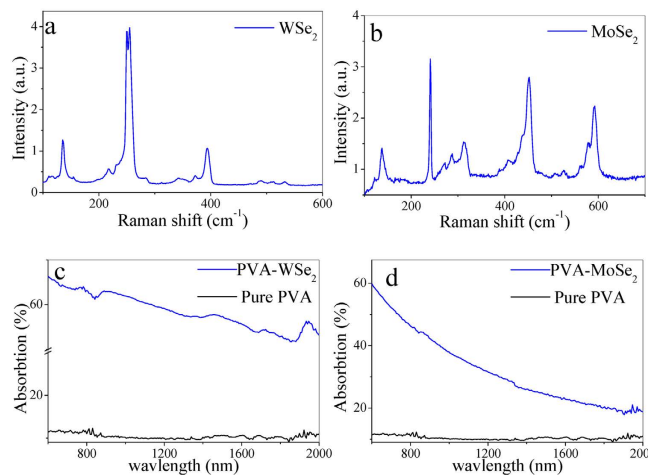


**Figure 8.** Raman spectra of (a) bulk WSe<sub>2</sub> and (b) bulk MoSe<sub>2</sub>. (c) Linear absorptions of PVA-WSe<sub>2</sub> film and (d) PVA-MoSe<sub>2</sub> film in comparison with pure PVA-film.

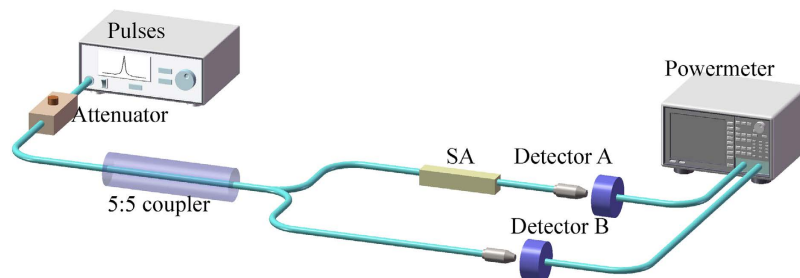


**Figure 9.** Schematic diagram of nonlinear optical characterization scheme.

similar lattice structures and photonic properties, we could deduce that sub-bandgap saturable absorption of WSe<sub>2</sub>/MoSe<sub>2</sub> nanosheets may be similar with that of the MoS<sub>2</sub> and WS<sub>2</sub> reported previously.

## Methods

**Preparation of WSe<sub>2</sub>/MoSe<sub>2</sub> nanosheets.** Before the liquid exfoliation, we identify the WSe<sub>2</sub>/MoSe<sub>2</sub> crystal by Raman spectroscopy using a 785 nm laser, as depicted in Fig. 8(a,b). The Raman spectra of bulk WSe<sub>2</sub> and bulk MoSe<sub>2</sub> agree well with the earlier findings<sup>54</sup>. The WSe<sub>2</sub>/MoSe<sub>2</sub> nanosheets are prepared by a liquid exfoliation method that consists of three steps. First, a solvent is prepared by mixing 50 mg sodium deoxycholate bile salt surfactant with 5 mL deionized water. Indeed, the solvent must be elaborately chosen to match the surface energy of the layered materials. Then, a piece bulk WSe<sub>2</sub>/MoSe<sub>2</sub> crystal (about 15 mg) is dropped into the prepared solvent, and the mixture is ultrasonic treated for 8 hours at power of 180 W. Note that impurities and defects are inevitable in the prepared sample, which may induce a small bandgap and thus a broadband optical response<sup>21</sup>. To remove the large aggregation, the dispersion is further centrifuged at 1000 rpm for 10 minutes and the 90% supernatant is collected for the next step of the experiment. The linear absorptions of PVA-WSe<sub>2</sub> film, PVA-MoSe<sub>2</sub> film, and pure PVA film are measured by a spectrometer (Hitachi UV4100). As shown in Fig. 8(c,d), the absorption coefficient decreases with the increase of wavelength from the visible to near-infrared band.

**Characterizing the nonlinear saturable absorption of WSe<sub>2</sub>/MoSe<sub>2</sub> SA.** The nonlinear saturable absorption property of SPF-WSe<sub>2</sub> SA, PVA-WSe<sub>2</sub> SA, SPF-MoSe<sub>2</sub> SA, and PVA-MoSe<sub>2</sub> SA are investigated separately with a balanced twin-detector measurement scheme. The illumination pulse is generated from a 1.55 μm EDF laser with the pulse repetition rate of ~25 MHz and the duration of ~400 fs. As shown in Fig. 9, the illumination pulse is divided equally by a coupler and the test sample is inserted in one branch. By adjusting the intensity of illumination pulse, the transmission of the SA as a function of incident power is obtained by comparing the output powers of two branches.

## References

- Geim, A. K. & Grigorieva, I. V. Van der Waals heterostructures. *Nature* **499**, 419–425 (2013).
- Zhang, S., Yan, Z., Li, Y., Chen, Z. & Zeng, H. Atomically thin arsenene and antimonene: semimetal-semiconductor and indirect-direct band-gap transitions. *Angew. Chem. Int. Ed. Engl.* **54**, 3112–3115 (2015).
- Chen, Y. *et al.* Mechanically exfoliated black phosphorus as a new saturable absorber for both Q-switching and mode-locking laser operation. *Opt. Express* **23**, 12823–12833 (2015).
- Martinez, A. & Sun, Z. Nanotube and graphene saturable absorbers for fibre lasers. *Nat. Photon.* **7**, 842–845 (2013).

5. Bonaccorso, F., Sun, Z., Hasan, T. & Ferrari, A. C. Graphene photonics and optoelectronics. *Nat. Photon.* **4**, 611–622 (2010).
6. Bao, Q. *et al.* Atomic-layer graphene as a saturable absorber for ultrafast pulsed lasers. *Adv. Funct. Mater.* **19**, 3077–3083 (2009).
7. Hendry, E., Hale, P. J., Moger, J., Savchenko, A. K. & Mikhailov, S. A. Coherent nonlinear optical response of graphene. *Phys. Rev. Lett.* **105**, 097401 (2010).
8. Lee, E. J. *et al.* Active control of all-fibre graphene devices with electrical gating. *Nat. Commun.* **6**, 6851 (2015).
9. Koppens, F. H. *et al.* Photodetectors based on graphene, other two-dimensional materials and hybrid systems. *Nat. Nanotechnol.* **9**, 780–793 (2014).
10. Pumera, M., Sofer, Z. & Ambrosi, A. Layered transition metal dichalcogenides for electrochemical energy generation and storage. *J. Mater. Chem. A* **2**, 8981 (2014).
11. Huang, X., Zeng, Z. & Zhang, H. Metal dichalcogenide nanosheets: preparation, properties and applications. *Chem. Soc. Rev.* **42**, 1934–1946 (2013).
12. Kang, J., Liu, W., Sarkar, D., Jena, D. & Banerjee, K. Computational study of metal contacts to monolayer transition-metal dichalcogenide semiconductors. *Phys. Rev. X* **4** (2014).
13. Li, Y. *et al.* Probing symmetry properties of few-layer MoS<sub>2</sub> and h-BN by optical second-harmonic generation. *Nano Lett.* **13**, 3329–3333 (2013).
14. Zhou, K. G. *et al.* Size-dependent nonlinear optical properties of atomically thin transition metal dichalcogenide nanosheets. *Small* **11**, 694–701 (2015).
15. Cunningham, G. *et al.* Solvent exfoliation of transition metal dichalcogenides: dispersibility of exfoliated nanosheets varies only weakly between compounds. *ACS nano* **6**, 3468–3480 (2012).
16. Kang, K. *et al.* High-mobility three-atom-thick semiconducting films with wafer-scale homogeneity. *Nature* **520**, 656–660 (2015).
17. Mak, K. F., McGill, K. L., Park, J. & McEuen, P. L. Valleytronics. The valley Hall effect in MoS<sub>2</sub> transistors. *Science* **344**, 1489–1492 (2014).
18. Cong, C. *et al.* Synthesis and optical properties of large-area single-crystalline 2D semiconductor WS<sub>2</sub> monolayer from chemical vapor deposition. *Adv. Opt. Mater.* **2**, 131–136 (2014).
19. Wang, K. *et al.* Broadband ultrafast nonlinear absorption and nonlinear refraction of layered molybdenum dichalcogenide semiconductors. *Nanoscale* **6**, 10530–10535 (2014).
20. Wang, K. *et al.* Ultrafast saturable absorption of two-dimensional MoS<sub>2</sub> nanosheets. *ACS nano* **7**, 9260–9267 (2013).
21. Wang, S. *et al.* Broadband few-layer MoS<sub>2</sub> saturable absorbers. *Adv. Mater.* **26**, 3538–3544 (2014).
22. Zhang, H. *et al.* Molybdenum disulfide (MoS<sub>2</sub>) as a broadband saturable absorber for ultra-fast photonics. *Opt. Express* **22**, 7249–7260 (2014).
23. Fu, X., Qian, J., Qiao, X., Tan, P. & Peng, Z. Nonlinear saturable absorption of vertically stood WS<sub>2</sub> nanoplates. *Opt. Lett.* **39**, 6450–6453 (2014).
24. Zhang, S. *et al.* Direct observation of degenerate two-photon absorption and its saturation in WS<sub>2</sub> and MoS<sub>2</sub> monolayer and few-layer films. *ACS nano* **9**, 7142–7150 (2015).
25. Mao, D. *et al.* WS<sub>2</sub> mode-locked ultrafast fiber laser. *Sci. Rep.* **5**, 7965 (2015).
26. Jung, M. *et al.* Mode-locked, 1.94-μm, all-fiberized laser using WS<sub>2</sub>-based evanescent field interaction. *Opt. Express* **23**, 19996–20006 (2015).
27. Liu, H. *et al.* Femtosecond pulse erbium-doped fiber laser by a few-layer MoS<sub>2</sub> saturable absorber. *Opt. Lett.* **39**, 4591–4594 (2014).
28. Du, J. *et al.* Ytterbium-doped fiber laser passively mode locked by few-layer Molybdenum Disulfide (MoS<sub>2</sub>) saturable absorber functioned with evanescent field interaction. *Sci. Rep.* **4**, 6346 (2014).
29. Zhao, G. *et al.* “Chemical weathering” exfoliation of atom-thick transition metal dichalcogenides and their ultrafast saturable absorption properties. *Adv. Funct. Mater.* **25**, 5292–5299 (2015).
30. Kumar, A. & Ahluwalia, P. K. Electronic structure of transition metal dichalcogenides monolayers 1H-MX<sub>2</sub> (M = Mo, W; X = S, Se, Te) from ab-initio theory: new direct band gap semiconductors. *Eur. Phys. J. B* **85**, 186 (2012).
31. Chen, B. *et al.* Q-switched fiber laser based on transition metal dichalcogenides MoS<sub>2</sub>, MoSe<sub>2</sub>, WS<sub>2</sub>, and WSe<sub>2</sub>. *Opt. Express* **23**, 26723–26737 (2015).
32. Luo, Z. *et al.* Nonlinear optical absorption of few-layer molybdenum diselenide (MoSe<sub>2</sub>) for passively mode-locked soliton fiber laser [Invited]. *Photonics Res.* **3**, A79–A86 (2015).
33. Woodward, R. I. *et al.* Wideband saturable absorption in few-layer molybdenum diselenide (MoSe<sub>2</sub>) for Q-switching Yb-, Er- and Tm-doped fiber lasers. *Opt. Express* **23**, 20051–20061 (2015).
34. Luo, Z. *et al.* Two-dimensional material-based saturable absorbers: towards compact visible-wavelength all-fiber pulsed lasers. *Nanoscale* **8**, 1066–1072 (2015).
35. Ruppert, C., Aslan, O. B. & Heinz, T. F. Optical properties and band gap of single- and few-layer MoTe<sub>2</sub> crystals. *Nano Lett.* **14**, 6231–6236 (2014).
36. Zhang, M. *et al.* Solution processed MoS<sub>2</sub>-PVA composite for sub-bandgap mode-locking of a wideband tunable ultrafast Er:fiber laser. *Nano Res.* **8**, 1522–1534 (2015).
37. Bonaccorso, F. & Sun, Z. Solution processing of graphene, topological insulators and other 2d crystals for ultrafast photonics. *Opt. Mater. Express* **4**, 63–78 (2013).
38. Yan, P. *et al.* A practical topological insulator saturable absorber for mode-locked fiber laser. *Sci. Rep.* **5**, 8690 (2015).
39. Zhao, C. *et al.* Ultra-short pulse generation by a topological insulator based saturable absorber. *Appl. Phys. Lett.* **101**, 211106 (2012).
40. Wang, F. *et al.* Wideband-tunable, nanotube mode-locked, fibre laser. *Nat. Nanotechnol.* **3**, 738–742 (2008).
41. Kobtsev, S., Kukarin, S., Smirnov, S., Turitsyn, S. & Latkin, A. Generation of double-scale femto/pico-second optical lumps in mode-locked fiber lasers. *Opt. Express* **17**, 20707–20713 (2009).
42. Liu, X., Cui, Y., Han, D., Yao, X. & Sun, Z. Distributed ultrafast fibre laser. *Sci. Rep.* **5**, 9101 (2015).
43. Sun, Z., Hasan, T. & Ferrari, A. C. Ultrafast lasers mode-locked by nanotubes and graphene. *Physica E: Low-dimensional Systems and Nanostructures* **44**, 1082–1091 (2012).
44. Sun, Z. *et al.* Graphene mode-locked ultrafast laser. *ACS nano* **4**, 803–810 (2010).
45. Lu, S. B. *et al.* Broadband nonlinear optical response in multi-layer black phosphorus: an emerging infrared and mid-infrared optical material. *Opt. Express* **23**, 11183 (2015).
46. Li, D. *et al.* Polarization and thickness dependent absorption properties of black phosphorus: new saturable absorber for ultrafast pulse generation. *Sci. Rep.* **5**, 15899 (2015).
47. Tang, D. Y., Zhao, L. M., Zhao, B. & Liu, A. Q. Mechanism of multisoliton formation and soliton energy quantization in passively mode-locked fiber lasers. *Phys. Rev. A* **72**, 043816 (2005).
48. Grudinin, A. B. & S. G. Passive harmonic mode locking in soliton fiber lasers. *J. Opt. Soc. Am. B* **14**, 144–154 (1997).
49. Pessina, E. M., Bonfrate, G., Fontana, F. & Lugiato, L. A. Experimental observation of the Risken-Nummedal-Graham-Haken multimode laser instability. *Phys. Rev. A* **56**, 4086–4093 (1997).
50. Woodward, R. I. *et al.* Tunable Q-switched fiber laser based on saturable edge-state absorption in few-layer molybdenum disulfide (MoS<sub>2</sub>). *Opt. Express* **22**, 31113–31122 (2014).
51. Banhart, F., Kotakoski, J. & Krasheninnikov, A. V. Structural defects in graphene. *ACS nano* **5**, 26–41 (2011).
52. Fominski, V. Y., Nevolin, V. N., Romanov, R. I. & Smurov, I. Ion-assisted deposition of MoS<sub>2</sub> films from laser-generated plume under pulsed electric field. *J. Appl. Phys.* **89**, 1449 (2001).



53. Hong, J. *et al.* Exploring atomic defects in molybdenum disulphide monolayers. *Nat. Commun.* **6**, 6293 (2015).  
54. Late, D. J., Shirodkar, S. N., Waghmare, U. V., Dravid, V. P. & Rao, C. N. Thermal expansion, anharmonicity and temperature-dependent Raman spectra of single- and few-layer MoSe<sub>2</sub> and WSe<sub>2</sub>. *Chemphyschem: a European journal of chemical physics and physical chemistry* **15**, 1592–1598 (2014).

### Acknowledgements

This work was supported by the National Natural Science Foundation of China (61575162, 61405161, 61505165, 61405162), the 973 Program (2012CB921900), and Fundamental Research Funds for the Central Universities (3102014JCQ01101).

### Author Contributions

D.M. designed the work, performed the experiments, and wrote the paper. X.S. and B.D. tested saturable absorption of the devices. X.C. measured the property of WSe<sub>2</sub> and MoSe<sub>2</sub> nanosheets. W.Z. and K.S. performed the part of experiment. T.P. and B.J. carried out the data analysis and revised the manuscript. D.Y. and J.Z. contributed to the scientific discussion and considerably improved the manuscript presentation. All authors discussed the results and substantially contributed to the manuscript.

### Additional Information

**Competing financial interests:** The authors declare no competing financial interests.

**How to cite this article:** Mao, D. *et al.* Erbium-doped fiber laser passively mode locked with few-layer WSe<sub>2</sub>/MoSe<sub>2</sub> nanosheets. *Sci. Rep.* **6**, 23583; doi: 10.1038/srep23583 (2016).



This work is licensed under a Creative Commons Attribution 4.0 International License. The images or other third party material in this article are included in the article's Creative Commons license, unless indicated otherwise in the credit line; if the material is not included under the Creative Commons license, users will need to obtain permission from the license holder to reproduce the material. To view a copy of this license, visit <http://creativecommons.org/licenses/by/4.0/>